Investigation of the Structural Deformation Mechanisms Induced by Microindentation in a Thermotropic Liquid Crystalline Copolyester Using Synchrotron X-ray Microdiffraction

Aurélien Gourrier,*,† Mari-Cruz García Gutiérrez,‡ and Christian Riekel§

Max-Planck Institute of Colloids and Interfaces, Biomaterials Department, D-14424 Potsdam, Germany, Instituto de Estructura de la Materia (CSIC), Macromolecular Physics Department, E−28006 Madrid, Spain, and European Synchrotron Radiation Facility, B.P. 220, F-38043 Grenoble Cedex, France

Received December 2, 2004; Revised Manuscript Received February 17, 2005

ABSTRACT: The structural changes induced by microindentation on thermotropic liquid crystalline copolyester fibers of 4-hydroxybenzoic acid (HBA) and 2-hydroxy-6-naphthoic acid (HNA) have been investigated by scanning X-ray microdiffraction techniques at the ESRF microfocus beamline (ID13). A phase transformation is observed upon deformation from a pseudohexagonal lattice (P_H) to two distinct orthorhombic phases (O_I, O_{II}). In addition, a strong texture is observed in the plastically deformed region as revealed by changes in the local orientation of the crystalline domains in the vicinity of the indenter tip and the appearance of reflections in specific directions only. This allows quantifying the extent of the deformation both across and along the fiber and also suggests the presence of complex structural processes occurring during indentation tests.

Introduction

Combined microindentation and synchrotron X-ray microdiffraction (μXRD) has recently been shown to yield a wealth of information concerning the deformation mechanisms in polymers occurring in the vicinity of the indenter tip.[1−3] As compared to other mechanical tests in which the whole sample is deformed, stresses applied in microindentation are concentrated in only a small region of the sample[4] (on the order of a few μm^3). Other advantages can be found in the absence of specific sample preparation as would be the case using electron microscopy techniques in that the high flux of synchrotron sources is well-suited for real-time studies on relatively bulky samples.[5,6]

The present study reports on results obtained using combined microindentation/μXRD applied to thermotropic liquid crystalline copolyesters of 4-hydroxybenzoic acid (HBA) and 2-hydroxy-6-naphthoic acid (HNA). Those have been extensively studied lately because of exceptional mechanical properties and, therefore, important potential industrial applications in high-performance materials.[7] The microstructure of these materials has been principally studied using electron microscopy[8−12] (EM) and small/wide-angle X-ray scattering (SAXS/WAXS)[13−24] techniques. The latter have also been used extensively to assess structural changes upon annealing[19−23] and during crystallization.[24] However, little is known concerning the structural processes involved in the deformation of such materials. The following article will show that combined μXRD and microindentation is a very useful tool to study such processes on a nanometer scale.

* Author to whom correspondence should be addressed. E-mail: gourrier@mpikg-golm.mpg.de. Telephone: +49 (0) 331 567 9451. Fax: +49 (0) 331 567 9402.
† Max-Planck Institute of Colloids and Interfaces.
‡ Instituto de Estructura de la Materia (CSIC).
§ European Synchrotron Radiation Facility.

Experimental Section

Materials. The samples investigated were polymer fibers of 4-hydroxybenzoic acid (HBA) and 2-hydroxy-6-naphthoic acid (HNA) monomers in a molar mass ratio of 73:27 HBA/HNA (Vectra A950). Both HBA and HNA are aromatic, which accounts for the extreme rigidity of the polymer fibers. This thermotropic copolyester was supplied by Goodfellow Cambridge Ltd. under the trade name Vectra. For the experiment, single fibers 23 μm in diameter were used as provided without additional preparation. The nature of the crystalline domains for this liquid crystalline polymer (LCP) has received particular attention[22,25,26] and is still an open matter of debate.[10,24] Nevertheless, crystallinity values of Vectra are generally reported in the range $\chi_c = 0.17-0.26$.[21,22]

Microindenter Setup. Single fibers were cut in length with microscissors and deformed using the dedicated microindenter setup described in detail elsewhere[1] according to the scheme shown in Figure 1. For this purpose, the sample was glued at both ends onto a diamond support and indented with a square-based diamond pyramid (Vickers indenter) pressed onto its surface under a given force F (mN), loading rate r (mN s^{-1}), and dwell time t (s).[4] After deformation at the required force, the sample was removed and glued at the end of a glass capillary, which is subsequently mounted on the X-ray setups. The indentation refers in the following to the plastically deformed region and can be viewed either parallel (as in Figure 3a) or normal to the direction of applied force shown by the solid and dotted arrows, respectively, in Figure 1. For reasons discussed below, in-situ experiments during indentation, although possible, were not tried in the present case.

Synchrotron Radiation Experiments. The experiments were carried out at the microfocus beamline (ID13) of the European Synchrotron Radiation Facility (ESRF).[6] A monochromatic beam of wavelength $\lambda = 0.097_6$ nm ($E = 12.78$ keV) was focused with an ellipsoid mirror and further reduced in size with either

10.1021/ma047509p CCC: $30.25
Published on Web 03/25/2005

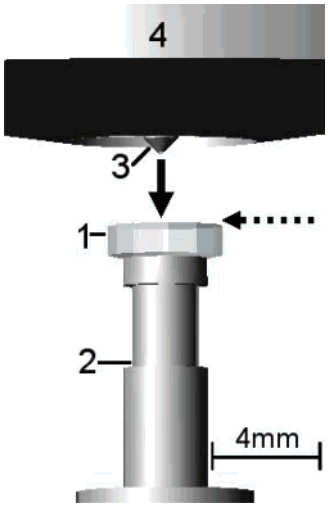

Figure 1. Simplified scheme of the indenter setup[1]. The sample is mounted on a diamond support (1−2) and deformed by the square-based diamond pyramid tip (3) of the Vickers indenter (4). The solid and dotted arrows indicate the direction of the force applied by the tip on the sample and its normal direction, respectively. Alternatively, the indenter can be exchanged with microscope objectives to select the region of interest.

a tapered glass capillary (3 μm) or collimators (5, 30 μm). A slow-scan 16-bit readout CCD detector (X-ray Associates (XRA)) with a 130-mm diameter X-ray converter screen and 2 K × 2 K pixels of 64.45 μm × 64.45 μm was used for data collection. The total exposure and readout time was about 15 s/frame. The sample-to-detector distance and the center of the detector were calibrated using an Ag-behenate standard.[27] Data were reduced and analyzed using the FIT2D software package.[28]

Results and Discussions

Phase Transition and Texture. Figure 2a shows a typical WAXS pattern collected with a 5-μm beam in an undeformed part of the fiber after background correction with a zoom of the equatorial peaks (Figure 2b). Because of the liquid crystalline nature of the copolyester, the pattern reveals a high degree of axial orientation while the presence of strong diffuse scattering indicates disordered packing in transverse directions.[29] The observation of off-equatorial sharp Bragg peaks also reveals, however, some degree of three-dimensional (3D) ordering. The maxima along the meridian were found to be aperiodic and were modeled by a random copolymer sequence.[14−16] Solid-state ^{13}C NMR supports such a random distribution with a weak tendency to form block copolymers.[30] These reflections were found, in our case, at q = 8.43, 18.61, and 27.67 nm^{-1} (d = 2.03, 3.02, and 6.64 Å, respectively), which is in good agreement with published values.[13,19−23] The radial profile in Figure 2c was obtained by integrating the intensity of the equatorial reflection along the azimuth direction within an annulus segment of ~3° as shown in Figure 2b. The asymmetry of the main peak is generally attributed to the presence of two strongly overlapping peaks that cannot be individually resolved, suggesting pseudohexagonal (P_H) symmetry[17−23] (orthorhombic lattice with $a = 3^{1/2}$ b). This phase observed at room temperature is generally believed to be a typical signature of compression-molded or as-extruded samples.[17−23] A fit was correspondingly achieved using

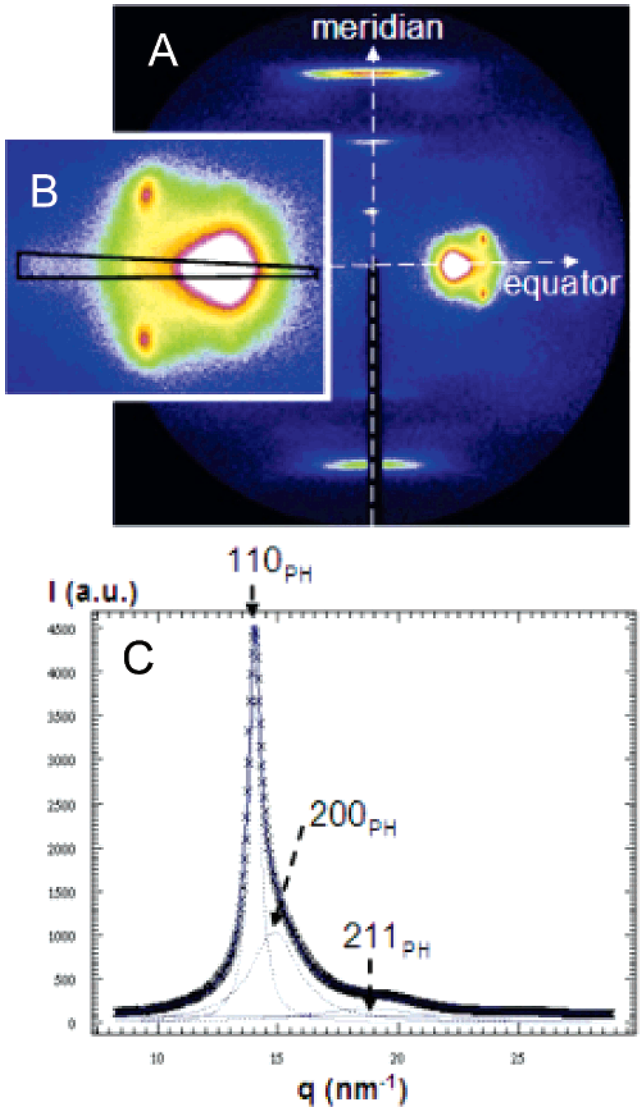

Figure 2. Typical WAXS pattern (a) of a Vectra fibre sample as provided. The most important features, aside from the diffuse scattering typical for liquid crystalline polymers (LCP), lay in the presence of three aperiodic maxima along the meridian and the presence of equatorial and off-equatorial peaks shown in more detail in (b). Radial profiles of the equatorial reflections in (c) were obtained by cake integration over a few azimuthal degrees. The fit was achieved using three Lorentzian functions and a first-order background polynomial, and the peaks were attributed to a pseudohexagonal phase. $q = 4\pi \sin(\theta)/\lambda(\text{nm}^{-1})$, where θ is the Bragg angle (°) and λ the X-ray wavelength (nm).

three Lorentzian functions and a first-order background polynomial. The two main peaks, indexed as 110_{PH} and 200_{PH}, were found respectively at q = 14.05 and 14.88 nm^{-1} (d_{110} = 4.45 Å, d_{200} = 4.22 Å, respectively), which is in good agreement with values found by other authors.[17−23] It should be noted that since the structure is essentially nonperiodic along the c-axis, the assignment of the l index of hkl reflections only refers, in our case, to the layer line number. The shoulder around q = 19 nm^{-1} is thought to be an extension of the 211_{PH} reflection which was found at q = 19.68 nm^{-1} (d = 3.19 Å).[17−23] For an orthorhombic lattice, the unit cell parameters are derived from $a = 2d_{200}$ and $b = 2d_{110}d_{200}/(4d_{200}^2 - d_{110}^2)^{1/2}$. The values of a = 8.90 Å and b = 5.23 Å are in good agreement with those found in the literature[19−21,23] and the ratio a/b = 1.70 is close to the ideal one of $a/b = 3^{1/2}$.

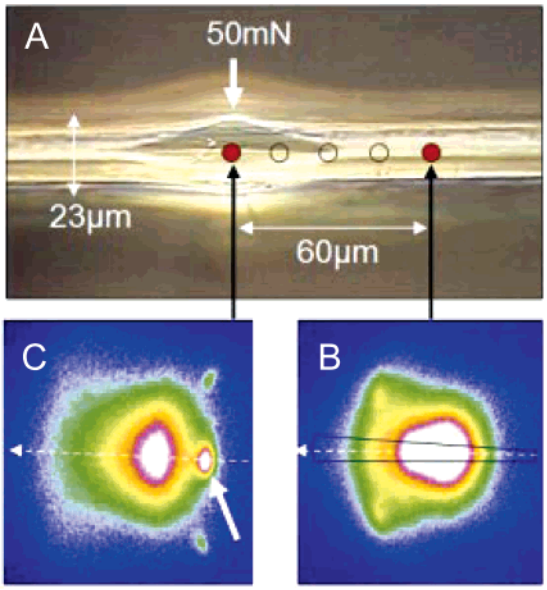

Figure 3. Optical microscopy image of an indented Vectra fiber (a) of 23 μm in diameter (50 mN at 5 mN s^{-1} for 10 s). Details of the equatorial peaks of WAXS pattern taken in an undeformed part (b) and in the center (c) of the indentation using a 5 μm beam. Note the appearance of an intense new peak indicated by the arrow.

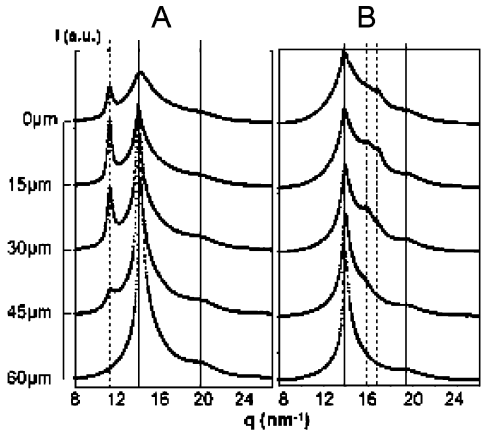

Figure 4. Radial profiles of the equatorial peaks taken at 15 μm intervals from the center of indentation (0 μm) with a 5 μm beam parallel (a) and normal (b) to the indentation direction (i.e., to the loading direction in which the force is applied). The peaks belonging to the original P_H phase are indicated by solid lines and those revealing the phase transition by dashed lines.

The details of the equatorial reflections from WAXS patterns collected in the centre of a 50 mN indentation (5 mN s^{-1}, 10 s) zone (Figure 3c) and at 60 μm distance (approximately the size of the indentation along the fiber axis as shown in Figure 3a) in an undeformed region (Figure 3b) reveal significant differences. In the deformed region, new peaks appear at lower q values, while others tend to fade. One particularly intense equatorial peak at $q = 11.42$ nm^{-1} (indicated by an arrow), which is not observed in undeformed zones, suggests a phase transition in the indented part of the fiber. The spatial extent of this phase transition is shown in more detail in Figure 4. The radial profiles of the equatorial reflections are displayed at 15 μm step intervals from the center of indentation along the fiber axis with the beam parallel (Figure 4a) or normal (Figure 4b) with respect to the loading direction of the indentation. The radial intensity profiles were obtained by integration as described above. The two main peaks of the initial phase indicated by the continuous lines also seem to be present in the indented zone although of weaker intensity. On the other hand, several new peaks indicated by dashed lines are seen to extend up to about 45 μm from the center of the indentation along the fiber axis. This suggests the coexistence of other phases in the indented region. In particular, the new equatorial peak observed in Figure 3c is clearly absent at 60 μm and gradually appears more intense relative to the total peak intensity when moving toward the center of the indentation in Figure 4a. On the other hand, this peak is totally absent from the profiles obtained in perpendicular direction to indentation, but two additional shoulders at $q \approx 16$ and 17 nm^{-1} indicated by dashed lines are seen to appear in the vicinity of the indentation.

Two conclusions can be drawn from these observations: (1) a partial phase transition takes place in the vicinity of the deformed region, and (2) the new phase shows a preferred orientation with respect to the direction of indentation. This can be described in more detail by recording the variation of the radial profiles of equatorial patterns obtained by rotating the indented fiber (50 mN) around its fiber axis in a 30 μm beam (so that the whole fiber is exposed) as described in Figure 5a. Figure 5b shows that the peak intensities are dependent upon fiber orientation, i.e., are a function of the angle ϕ between the beam direction and indentation directions. In particular, the equatorial peak at $q = 11.42$ nm^{-1} is most intense at $\phi = 0°$ and quasi-extinct at $\phi = 90°$ (beam respectively parallel and normal to indentation direction). Such variation in the WAXS profiles clearly reveals a strong 3D texture of the crystalline domains in the indented zone.

Indexation of the new peaks observed is not straightforward but is facilitated by several considerations. First, most phase transitions in Vectra A950 reported in the literature occurred during annealing studies in which specific attention is given to the attribution of the equatorial peaks.[17−24] On the basis of electron diffraction studies on polyHBA homopolymer,[31] WAXS data obtained from compression-molded or as-extruded samples at room temperature are usually indexed according to the P_H lattice indicated above. Upon annealing, the 110_{PH} and 200_{PH} peaks are found to shift respectively to lower and higher q values. This peak separation has been associated with a transition to an orthorhombic lattice (O_I). Although no clear splitting of the overlapping $110/200_{PH}$ equatorial peak is observed in our case, the presence of weak off-equatorial peaks tend to indicate that an O_I phase is indeed present, although representing only a very small volume fraction of the crystalline material. These were thus indexed as 111_{OI} in Figure 6b according to detailed descriptions given by some authors.[21] According to those results, the $110/200_{PH}$ and $110/200_{OI}$ would still overlap and could not be distinguished. Second, other peaks of stronger intensity cannot be indexed as belonging to the O_I phase. Figure 6c shows a difference pattern obtained by subtraction of a pattern taken in an undeformed region (Figure 6a) from that of an indented one (Figure 6b) in a parallel orientation ($\phi = 0°$). At least three peaks (in white) including, in particular, the peak on the equator at $q = 11.42$ nm^{-1} ($d = 5.50$ Å), suggest an additional phase (or several) different from O_I. This could belong to yet another orthorhombic modification

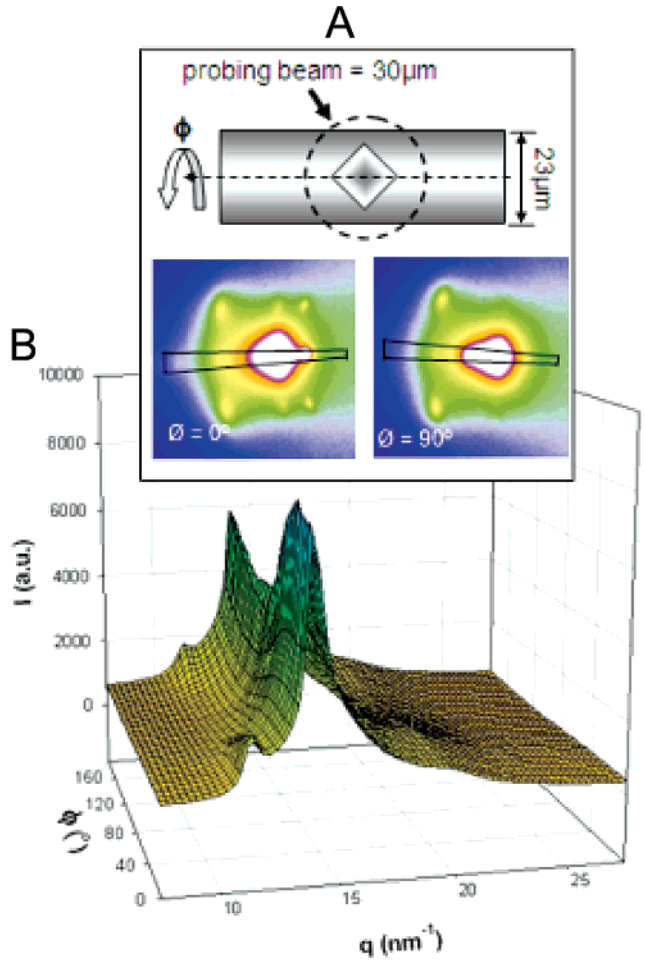

Figure 5. Radial profiles of the equatorial peaks as a function of the angle ϕ between the beam and the direction of indentation upon rotation of the fiber with respect to its main axis (b) in a 30 μm beam (the whole fiber is in this case exposed) as seen in (a). Details of the equatorial patterns at $\phi = 90°$ and $\phi = 0°$ (normal and parallel to indentation direction, respectively).

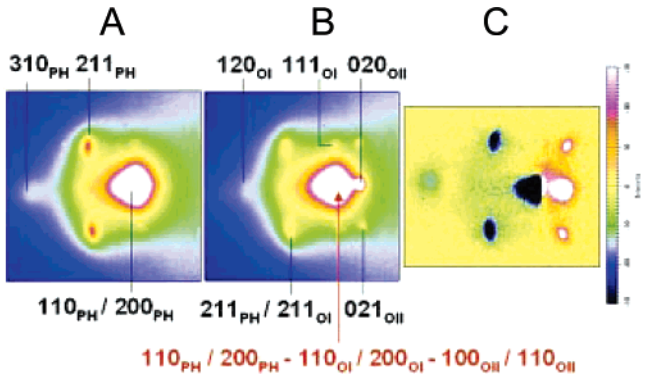

Figure 6. Indexation of the equatorial peaks in undeformed (a) and indented (b) regions belonging to a pseudohexagonal phase (P_H) and two orthorhombic modifications (O_I and O_{II}). Difference pattern (c) emphasizing the peaks belonging to the O_{II} phase in white. P_H, O_I, and O_{II} are referred to as III, I, and II, respectively, in refs 20 and 31 and to P_H, O′, and II, respectively, in refs 21 and 22.

O_{II} (020_{OII}), which is also observed in the HBA homopolymer[31] and which few authors also suggest is as a result of annealing.[19,21] The other off-equatorial peak in Figure 6c, $q = 11.60$ nm^{-1} ($d = 5.42$ Å) should, in this case, also be attributed to this phase (121_{OII}). A last step must, therefore, be taken concerning the equatorial

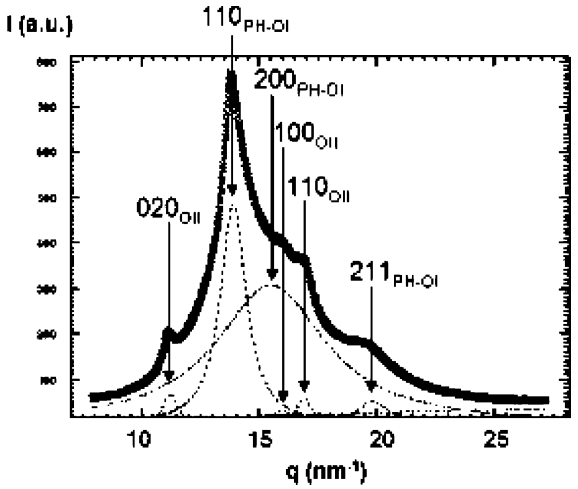

Figure 7. Details of the fitting of the average equatorial profile through rotation in a 50 mN indentation. Fitting was achieved using three Lorentzian functions to account for the indiscernible P_H and O_I phases, three for each peak of the O_{II} phase, and a first-order background polynomial. The 211_{PH-OI} is, in fact, an extension of this peak on the equator.

peaks indicated by dashed lines in Figure 4b ($\phi = 90°$) that strongly overlap with the main peak but can still be resolved in some cases. Figure 7 shows the azimuthally averaged radial profile from $\phi = 0-90°$ at 15 μm from the center of indentation where the O_{II} peaks appear most intense (shown in Figures 4 and 5). Fitting was achieved using single Lorentzian functions to account for the same peaks of both the P_H and O_I phases (110, 200, and 211), which cannot be individually resolved as mentioned above. This assumption is based on the fact that only a minor fraction of the O_I phase should contribute to the total intensity as observed by the very weak intensity of the 111_{OI} peaks as already mentioned. Three additional Lorentzian functions were used to account for the 020_{OII} and extra reflections along with a first-order background polynomial. Although rarely reported in the literature in the case of this copolyester, the results obtained on HBA indicate the existence of two extra equatorial peaks for the O_{II} phase that correspond well with those found in our case at $q = 16$ and 17 nm^{-1}, which were consequently indexed as 100_{OII} and 110_{OII}. The indexation proposed in Figure 6 is, therefore, based on the above considerations, although definite conclusions regarding the exact structure of this new crystalline phase would require indexing a larger number of reflections typically absent in such LCPs. It is also worth noting that the weak fraction of the O_I phase observed in undeformed fibers could indicate a possible skin-core effect. Because of limited resolution in beam-size, this was not investigated, although recent experiments tend to show this could be possible in a near future.[34]

Influence of the Indentation Force on the Phase Transition. To evaluate the dependence of the extent of the phase transformation on the applied force, WAXS patterns were collected in fibres indented at 10 and 30 mN (at, respectively, 1 and 3 mN s^{-1} for 10 s) as a function of ϕ in the same way as for the 50 mN indentation described above. It is important at this stage to note that the radial profiles in which the peaks from the O_{II} phase appear most clearly and shown in Figures 4, 5, and 7 were obtained from a WAXS pattern obtained using a 5 μm beam. This implies that, when calculating the average diffraction pattern necessary to quantify the

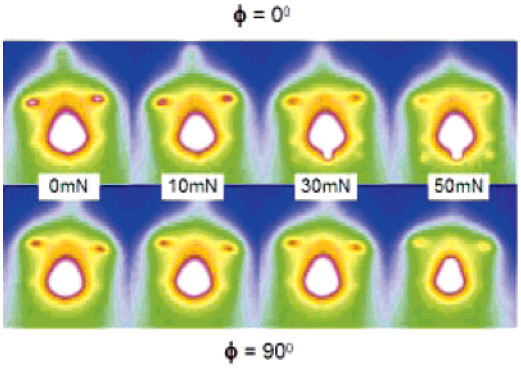

Figure 8. Evolution of the equatorial peaks as a function of the indentation force applied for $\phi = 0°$ (parallel) and $\phi = 90°$ (normal direction to indentation).

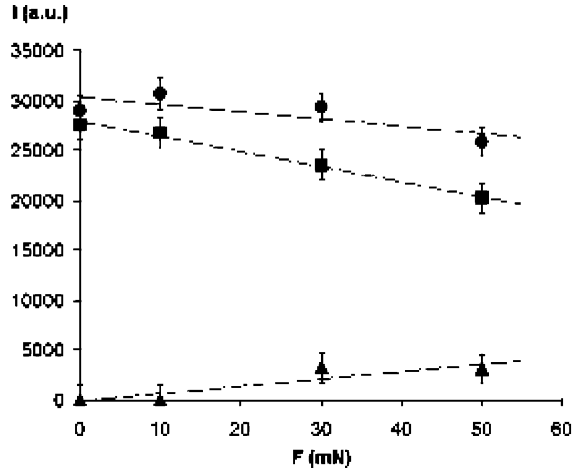

Figure 9. Integrated intensity of the total equatorial reflection (solid dots), the 110/200 P_H-O_I peaks (squares), and 020/100/110 O_{II} peaks (triangles) as a function of indentation force.

phase transformation due to orientational anisotropy, the volume fraction of the phase present in the center of the fiber (sphere of 5 μm diameter) will be overestimated, emphasizing the effects occurring upon indentation. This has allowed indexing of the different peaks of the new phases, but quantitative evaluation of the amount of phase formed during the deformation process requires that the whole fiber is exposed to the beam. A 30 μm beam was thus used to expose the whole fiber. The equatorial reflections are shown for the different forces at $\phi = 0$ and 90° in Figure 8. One can notice that the 020_{OII} peak appears gradually as the force applied increases. Furthermore, the anisotropy of crystalline orientation, reflected from the differences between patterns at $\phi = 0$ and 90°, also seems to be an increasing function of the force. The average radial profiles were obtained and fitted as previously. Figure 9 shows the evolution of the total integrated intensities of the different fitted peaks of the O_{II} and P_H/O_I and of the whole peak as a function of the indentation force. The latter tends to suggest a decrease in total crystallinity of ~15% at 50 mN, which is not very high considering the importance of the deformation induced (see Figure 3a). Also, the proportion of O_{II} phase relative to that of P_H/O_I is clearly seen to increase with the force (2.5, 8.4, and 15%, respectively, at 10, 30, and 50 mN).

Crystalline Orientation and Phase Distribution. To define more accurately the spatial extent of the phase transition, a fiber indented at 50 mN (5 mN s^{-1}, 10 s) was scanned with a 2 μm beam as described in Figure 10a. The sample was oriented with the indentation parallel ($\phi = 0°$) and normal ($\phi = 90°$) to the probing beam. Figure 10b shows a composite image of the WAXS equatorial reflections at each scan position about the indented zone. Details of the scan (Figure 10c, d) indicate a tilting of the equatorial reflections in a number of patterns, which reveals a change in the local fiber orientation with respect to the macroscopic fiber axis. This can be quantified by a vector L (Figure 10d), for which the length is taken to be proportional to the azimuthal fwhm of the $110_{PH/OI}$ equatorial peak and direction is defined by the relative azimuthal angle of tilt of the local meridian with respect to the fiber axis outside the deformed zone (α). The length is, therefore, approximately correlated with the orientation distribution of crystalline domains probed by the beam about the local fiber axis (meridian). A vector plot at each scan position is shown in both parallel (Figure 11a) and normal (Figure 11b) directions with respect to this indentation. The fwhm of the main equatorial peak (vector length) were normalized to account for the convolution of beam size with the shape of the fiber. Also, for visualization purposes, the tilt in azimuthal angle (vector direction), which is found to be at maximum on the order of 5°, is enhanced by a coefficient factor to stress the effect of the deformation. The indentation position is also represented at a slight offset with respect to the fiber axis. It can be seen from these plots that the crystalline domains in this LCP tend to orient under the stress field developed under the indenter. Because of the rigid rod nature of this particular LCP, this implies that the molecules tend to align along the faces of the indenter. Also, the vector length is found to increase in the indentation zone, which corresponds to an azimuthal broadening and thus a wider distribution in molecular orientation, although of minor importance (less than 1.5° in azimuth at maximum in this case). A plot of the intensity of 020_{OII} at each scan position is also shown in Figure 11c, d and allows visualizing the extent of the phase change. In principle, a 3D reconstruction of the extent of phase transformation should be feasible from similar scans taken at different angles. One practical conclusion in this case is that an analysis of the changes in orientation observed in the WAXS patterns was sufficient to determine the relative position of the indentation on the fiber (which is confirmed in our experiment by visual examination). Also, this experiment shows that one can determine the extent of the plastic deformation within the material (±40 μm) within the precision given by the beam size, providing no overlapping occurs (in which case, the spatial resolution can be increased by deconvolution operations).

Origin and Mechanisms of the Phase Transition. The phase transformation in Vectra occurring upon heating is generally explained as an evolution of the frozen conformational disorder in as-extruded fibers that pack in a pseudohexagonal lattice (P_H) into energetically more stable conformations where the aromatic planes are better correlated.[19,20,24] Hence, molecular chains with an ordered conformation adopt a 2-fold symmetry in which the HNA units are built in as imperfections in an orthorhombic packing[24] (O_I). It is, therefore, striking that in our case, the most important new phase induced by indentation is O_{II} rather than O_I. It is also important to note that the presence of 111_{OI} peaks was

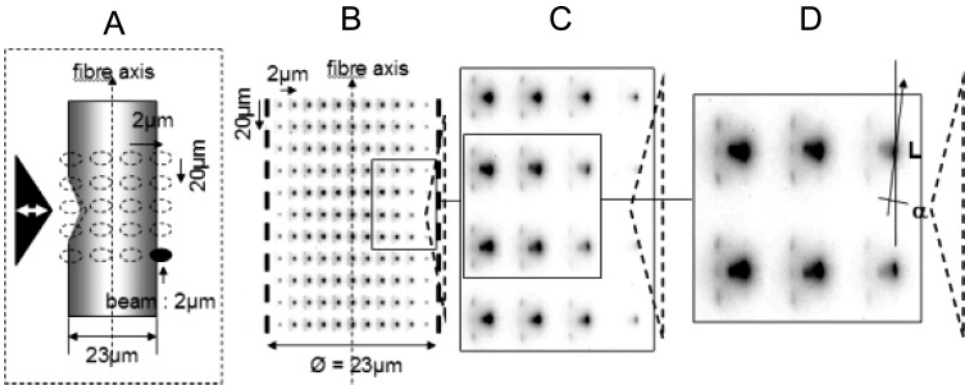

Figure 10. Scheme of a scanning microdiffraction experiment (a) on a Vectra fiber using a 2 μm beam in normal direction to indentation ($\phi = 90°$). Composite image of the equatorial reflections at each scan point in direction normal to indentation (b). Details of the indentation zone showing a tilt of the WAXS pattern (c) and (d).

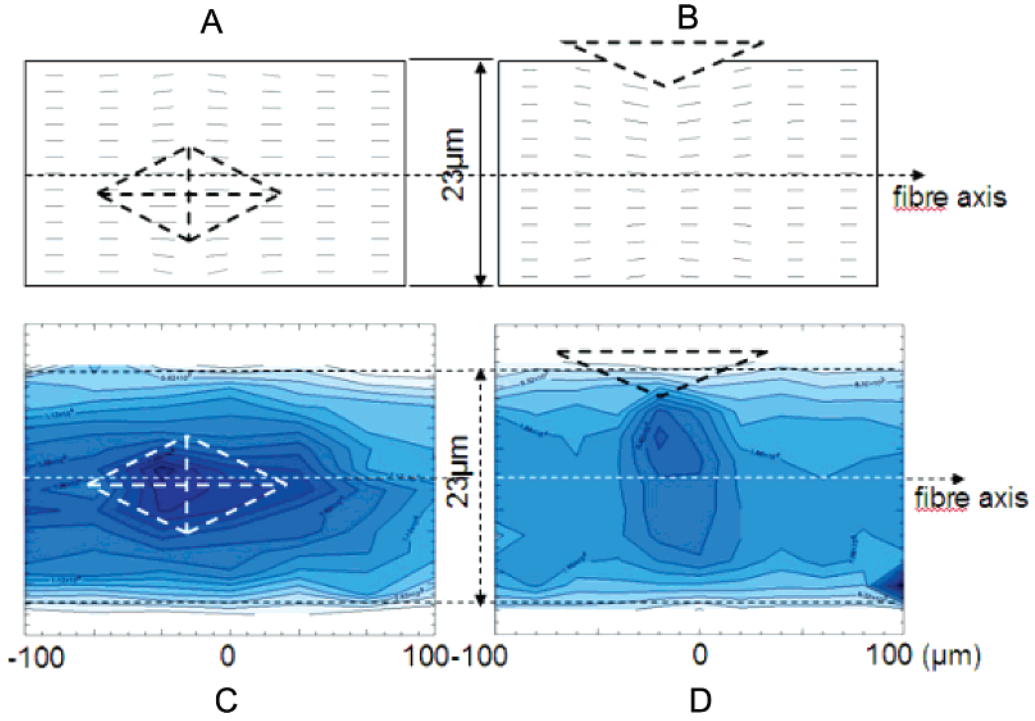

Figure 11. Vector plots of the local crystalline orientation in parallel (a) and normal (b) direction to indentation. The vector length is proportional to the fwhm of the 110_{PH-OI} reflection, and direction is given by the tilt of the meridian with respect to the macroscopic fiber axis. Map of the 020 O_{II} integrated intensity (c) and (d) in the same direction as (a) and (b), showing the extent of the phase transformation.

also noticed in undeformed samples, suggesting that a weak proportion of this phase is always present in as-extruded samples. Furthermore, a recent uniaxial compression study of Vectra[32] on as-extruded samples in which the force is applied normal to the extrusion direction (similar to our case) did not reveal a clear phase transition of the initial P_H phase even at strains as high as 50%. However, the same experiment repeated on an annealed sample shows a partial transition from O_I (obtained from P_H through annealing) to O_{II}, which is found to be a function of the applied compressive stress and is thought to be a shear-induced martensitic transition.[32] This differs from our observations of a direct transition from P_H to O_{II}. Nevertheless, several points should be emphasized here that could at least partially account for those differences. Our study suggests that the O_{II} phase formed upon deformation was strongly textured. This implies that the intense 020_{OII} peak, which can clearly be resolved and is hence most likely to be observed, appears strongest in parallel direction to indentation and quasi-extinct at 90°. As a result, the most likely configuration in which this phase will be observed is thus when the X-ray beam is parallel to the direction in which the force is applied. The case in which the WAXS pattern is collected by rotating the sample in the beam is, in this respect, the less favorable, as this would further average out the 020_{OII} peak. Recent in-situ microindentation studies performed in the usual configuration where the beam is normal to the loading direction[1] did not allow us so far to observe the formation of this phase. Also, the phase transition is only partial (15% at 50 mN), and its extent is limited to the vicinity of the indenter tip. It will, therefore, be better resolved when the beam probes mainly a zone where this phase is formed which requires the use of microbeams. In addition, it should be pointed out that the stress field developing under the indenter is quite complex.[4,33] In light of the present results, one could, therefore, not exclude that there could be a formation of a temporary O phase formation ($P_H \rightarrow O_I \rightarrow O_{II}$)

during microindentation. Finally, the influence of the molecular weight (degree of polymerization) of the material on the phase transition should be investigated, as it was shown to have a strong influence on the homopolymer HBA.[31]

Conclusions

The present study showed that microindentation performed on a Vectra fiber resulted in a complex partial phase transformation in the vicinity of the indenter tip. The results found using μXRD with beam sizes in the range 2−30 μm revealed that the initial pseudohexagonal lattice of the crystalline part of the material transforms into an orthorhombic phase. Using the 2 μm beam, it was possible to map the extent of the transition by scanning μXRD. The same technique also allowed resolving the local orientation of the crystalline domains with a spatial resolution defined by the beam size. Those are, therefore, shown to orient parallel to the faces of the indenter as suggested in previous studies on other polymer fibers.[1] This texture is particularly evidenced by the differences in WAXS patterns taken in both parallel and normal direction to the indentation upon rotating the fiber about its main axis.

Acknowledgment. The results reported are part of the thesis work of A.G. at the Université J. Fourier in Grenoble. We thank J. Lange, L. Lardière, J. Meyer, H. Gonzalez ,and M. Burghammer (ESRF) for their help in developing the microindenter setup. M.C.G.G. is grateful to the European Community for the support of this research by a Marie Curie Fellowship of the European Community program "Improving Human Research Potential and the Socio-Economic Knowledge" under the contract number HPMF-CT-2000-00892.

References and Notes

(1) Gourrier, A.; García-Gutiérrez, M. C.; Riekel, C. *Macromolecules* **2002**, *35*, 8072−8077.
(2) García-Gutiérrez, M. C.; Gourrier, A.; Riekel, C. *J. Macromol. Sci., Phys.* **2004**, *43*, 267−277.
(3) Riekel, C.; García-Gutiérrez, M. C.; Gourrier, A.; Roth, S. *Anal. Bioanal. Chem.* **2003**, *376*, 594−601.
(4) Baltà-Calleja, F. J.; Fakirov, S. In *Microhardness of Polymers*; Cambridge University Press: Cambridge, 2000.
(5) Elsner, G.; Riekel, C.; Zachmann, H. G. In *Advances in Polymer Science*; Kausch, H., Ed.; Springer-Verlag: Heidelberg 1985; pp 67−124.
(6) Riekel, C. *Rep. Prog. Phys.* **2000**, *63*, 233−262.
(7) Calundann, G. W.; Jaffe, M. *Proc. Robert A. Welch Found. Conf. Chem. Res.* **1982**, *26*, 247.
(8) Donald, A. M.; Windle, A. H. *J. Mater. Sci.* **1983**, *18*, 1143−1150.
(9) Spontak, R. J.; Windle, A. H. *J. Mater. Sci.* **1990**, *25*, 2727−2736.
(10) Plummer, C. J. G.; Kausch, H. H. *Polymer* **1997**, *38*, 1745−1748.
(11) Sawyer, L. C.; Grubb, D. T. In *Polymer Microscopy*; Chapman & Hall: London, 1996.
(12) Taylor, J. E.; Romo-Uribe, A.; Libera, M. R. *Polymer* **2002**, *43*, 1641−1648.
(13) Gutierrez, G. A.; Chivers, R. A.; Blackwell, J.; Stamatoff, J. B.; Yoon, H. *Polymer* **1983**, *24*, 937−942.
(14) Biswas, A.; Blackwell, J. *Macromolecules* **1988**, *21*, 3146−3152.
(15) Biswas, A.; Blackwell, J. *Macromolecules* **1988**, *21*, 3152−3158.
(16) Biswas, A.; Blackwell, J. *Macromolecules* **1988**, *21*, 3158−3164.
(17) Stamatoff, J. B. *Mol. Cryst. Liq. Cryst.* **1988**, *110*, 75−91.
(18) Antipov, E. M.; Volegova, I. A.; Godovskii, Y. K.; Stamm, M.; Fischer, E. W. *J. Macromol. Sci.* **1996**, *B35*, 591−614.
(19) Kaito, A.; Kyotani, M.; Nakayama, K. *Macromolecules* **1990**, *23*, 1035−1040.
(20) Sun, Z.; Cheng, H. M.; Blackwell, J. *Macromolecules* **1991**, *24*, 4162−4167.
(21) Wilson, D. J.; Vonk, C. G.; Windle, A. H. *Polymer* **1993**, *34*, 227−237.
(22) Hanna, S.; Lemmon, T. J.; Spontak, R. J.; Windle, A. *Polymer* **1992**, *33*, 3−10.
(23) Flores, A.; Ania, F.; Balta-Calleja, F. J.; Ward, I. M. *Polymer* **1993**, *34*, 2915−2920.
(24) Langelaan, H. C.; Posthuma de Boer, A. *Polymer* **1996**, *37*, 5667−5680.
(25) Windle, A. H.; Viney, C.; Golombok, R.; Donald, A. M.; Mitchell, G. R. *Faraday Discuss. Chem. Soc.* **1985**, *79*, 55−72.
(26) Blackwell, J.; Biswas, A.; Gutierrez, G. A.; Chivers, R. A. *Faraday Discuss. Chem. Soc.* **1985**, *79*, 73−84.
(27) Blanton, T. N. et al. *Powder Diffr.* **1995**, *10*, 91−95.
(28) Hammersley, A. P. *ESRF Internal Report*; Report No. ESRF97 HA02T; European Synchrotron Radiation Facility: Grenoble Cedex, France, 1997.
(29) Blackwell, J., Chivers, R. A., Gutierrez, G. A.; Biswas, A. *J. Macromol. Sci.* **1986**, *B24*, 39−59.
(30) Muhlebach, A.; Johnson, R. D.; Lyerla, J.; Economy, J. *Macromolecules* **1988**, *21*, 3115−3117.
(31) Lieser, G. *J. Polym. Sci.* **1983**, *21*, 1611−1633.
(32) Salahshoor-Kordestani, S.; Hanna, S.; Windle, A. H. *Polymer* **2000**, *41*, 6619−6626.
(33) Rikards, R.; Flores, A.; Kushnevski, V.; Baltà-Calleja, F. J. *J. Comput. Mater. Sci.* **1998**, *11*, 233−244.
(34) Riekel, C.; Davies, R. *Curr. Opin. Colloid Interface Sci.* **2004**. In press.

MA047509P